# Aligned Carbon Nanotube-Based Sensors for Strain Monitoring of Composites

Ana Raquel Santos, Luís Amorim, João Pedro Nunes, Alexandre F. Silva, and Júlio C. Viana

***Abstract*—This paper presents a proof of concept of an aligned carbon nanotube (CNT) based strain sensor tested on the surface of a conventional aeronautic laminate. Two type of strain sensors were produced, type S and type T, in which the CNT alignment was parallel (Y) and transversal (X) to strain direction, respectively. Their electrical resistance response was thoroughly evaluated during cyclic tensile tests. Despite some disparities of the relative electrical resistance behavior in specific strain cycles, probably due to one-off interferences in the CNT conductive mechanism, the obtained gauge factor (GF) values were quite stable. Also, the electrical resistance anisotropy was evaluated and its opposite behavior when the samples were strained in Y- and X-directions may be used as strain direction indicator. Being able to quantify and indicate strain direction with just one 10 × 10 mm CNT patch, this sensor has proven to be suitable for strain sensing applications, namely for structure health monitoring of advanced composites.**

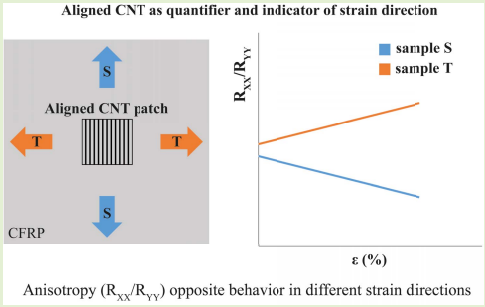


***Index Terms*— Aligned carbon nanotubes, electrical anisotropy, strain sensor, structure health monitoring.**

## I. Introduction

NOT long after their discovery, carbon nanotubes (CNT) have been used in all kind of fields, industry, energy, aerospace and electronics, among others, mainly due to their unique mechanical, electrical and chemical properties. Their enormous potential for sensing applications made researchers turn to CNT as structural health monitoring solutions. Moreover, their incorporation into thin films for structural composite monitoring is already a common approach among researchers [1], [2].

Manuscript received March 4, 2021; revised March 25, 2021; accepted March 31, 2021. Date of publication April 5, 2021; date of current version June 30, 2021. This work was supported in part by the Project "Introduction of Advanced Materials Technologies Into New Product Development for the Mobility Industries—IAMAT," under the MIT-Portugal program exclusively financed by Fundação para a Ciência e Tecnologia "FCT" under Grant MITP-TB/PFM/0005/2013 and in part by the North Portugal Regional Operational Programme (NORTE 2020) under the Portugal 2020 Partnership Agreements through the European Regional Development Fund (ERDF) Project "Technologies for Sustainable and Smart Innovative Products (TSSiPRO)" under Grant NORTE-01-0145-FEDER-000015. The associate editor coordinating the review of this article and approving it for publication was Dr. Cheng-Sheng Huang. *(Corresponding author: Ana Raquel Santos.)*

Ana Raquel Santos, Luís Amorim, João Pedro Nunes, and Júlio C. Viana are with the Institute for Polymers and Composites (IPC), University of Minho, 4804-533 Guimarães, Portugal (e-mail: arrsantos90@gmail.com; luis.amorim@dep.uminho.pt; jpn@dep.umniho.pt; jcv@dep.uminho.pt).

Alexandre F. Silva is with the Center for MicroElectroMechanical Systems (CMEMS), University of Minho, 4804-533 Guimarães, Portugal (e-mail: asilva@dei.uminho.pt).

Digital Object Identifier 10.1109/JSEN.2021.3070927

Within this context, the CNT can be used in the form of Buckypapers [3]–[6], nanocomposites [7]–[11] or vertically aligned forests (VA-CNT) [12], [13], despite the numerous drawbacks regarding dispersion, agglomeration and bundling, which strongly affect their electrical and mechanical properties. Particularly, the Buckypapers present weaker mechanical properties, having a small deformation at break; nanocomposites can have many problems during the production process due to the needed balance between the CNT percentage, which can be high, easy handling or/and manufacturing and required electrical conductivity; whereas VA-CNT proved to have a heterogeneous resin impregnation with some structure damage. Some of these difficulties can be mitigated by CNT functionalization, e.g., increase the affinity between the CNT and the matrix, improving dispersion or helping to maintain a structure, resulting in an increased electrical conductivity. However, this process itself has its own challenges and may add unnecessary complexity to the production process.

Not only the CNT alignment or realignment can diminish the problems above mentioned, but also can yield interesting and advantageous electrical and mechanical properties. A CNT-based solution can be effectively aligned by an electric field, however with a particular restraint, i.e., at some current levels the CNT agglomeration increases [14], [15]. Other alignment techniques are mechanical stretching [16], [17] or directly drawn the CNT from a vertically aligned forest to a Buckypaper form [18], [19], which can definitely damage the nanotube structure. More recently, the mechanical knock down

of VA-CNT forests to obtain a reoriented CNT patch showed to be a simple and efficient process [20], [21], with application in strain monitoring [22]. Despite all these progresses regarding CNT incorporation into thin films for structural composite monitoring, most of the reports published in literature do not test the CNT based sensors in conventional laminates with real applicability.

In our previous work [22], the electrical behavior of knocked down VA-CNT/polyimide (PI) strain sensors were study, showing good sensitivity to strain. Also, regarding the CNT patch conduction mechanism, it was proposed that the electrical resistance of the patch mainly depends on the number of CNT-CNT junctions (conduction through contact) at small deformations or/and CNT-CNT distances (conduction through tunneling effect) at higher deformations. These mechanisms (nano-scale) share the same basic principles explored by other authors [10], [11] (micro-scale at high deformation) regarding CNT conduction pathway.

In this work, in order to test the real applicability in composite monitoring, the aligned CNT patch is directly transferred to the surface of a carbon fiber reinforced polymer (CFRP) with a conventional aeronautic layout laminate, and then subjected to low cyclic tensile test. During these tests, the relative electrical resistance and electrical resistance anisotropy of the CNT sensing patch were evaluated. The sensors tested on the CFRP surface proved to be sensitive to strain and suitable for composite monitoring applications. Also, the electrical resistance anisotropy behavior proved to be a good indicator of the strain direction.

## II. Materials and Methods

### A. Aligned CNT Samples Production

Vertically aligned CNT (VA-CNT) forests of 10 mm x 10 mm size, were grown by chemical vapor deposition with a gas mixture of hydrogen/helium/ethylene and temperature of 750 °C. The detailed process is described elsewhere [23].

The VA-CNT were mechanically knocked down onto polyimide films, PI (75 $\mu$m Kapton MP film). An apparatus, composed by a metallic rod and two 3D printed supports, was developed for this purpose. Detailed description can be found elsewhere [22].

### B. Aligned CNT/CFRP Production

The knocked down CNT were transferred onto the surface of a CFRP plate with dimensions 250 mm x 25 mm x 4 mm. The CFRP, composed by twenty-eight layers of unidirectional carbon fiber fabrics (Dynanotex HS 24/150 DLN2, from G. ANGELONI s.r.l., Italy), with standard layup $[0/45/90/-45/45/-45/0]_{2s}$, were impregnated with Biresin® CR83 epoxy resin (from Sika®) by vacuum bag infusion. For the electrical resistance measurements, a silver conductive epoxy adhesive (8330S from MG Chemicals) was used as electrode of the CNT patch (Fig. 1).

### C. Electrical Resistance Measurements

For the electrical resistance measurements, an adaptation of the Van der Pauw method for anisotropic conductors [24], [25]

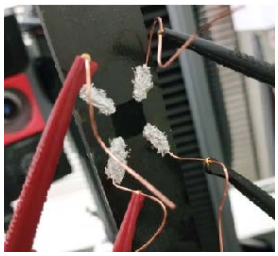

Fig. 1. Knocked down CNT/CFRP sample.

was developed using MATLAB software (R2018a, Mathworks, Natick, Massachusetts, USA). The adaptation consists in the conformal transformation from isotropic to anisotropic conductor resulting in (1), from which the $R_{yy,\square}/R_{xx,\square}$ value is obtained.

$$\frac{a/2}{b\sqrt{R}_{yy,\square}/R_{xx,\square}} = \frac{\int_0^{\pi/2} \frac{d\varphi}{\sqrt{1-k^2(\sin\varphi)^2}}}{\int_0^{\pi/2} \frac{d\varphi}{\sqrt{1-(\sin\varphi)^2+k^2(\sin\varphi)^2}}} \quad (1)$$

where a and b ar the CNT's patch square dimensions, which initially are $a_0 = b_0 = 10$ mm. These dimensions vary with the applied deformation. In the case of the tensile test: $a = a_0 + \Delta l$ in the strain direction ($\Delta l$ is the elongation recorded by an optical extensometer), and, in the transverse direction, $b = b_0 - \upsilon\varepsilon l_{t0}$, considering the Poisson effect, where $\upsilon$ is the Poisson ratio, $\varepsilon$ is the mechanical strain and $l_{t0}$ is the initial width of the CFRP. $R_{yy,\square}$ and $R_{xx,\square}$ are the resistances in the parallel direction (Y) and the transverse direction (X) with respect to the CNT alignment and $k$is an experimental value which depends on the injected currents ($I_{AB}$ and $I_{AD}$) and measured voltages ($V_{DC}$ and $V_{BC}$).

From an adaptation of the Van der Pauw equation [24] (2), the sheet resistance value, $R_s$, is obtained:

$$e^{-\pi R_{vertical}/R_s} + e^{-\pi R_{horizontal}/R_s} = 1 \quad (2)$$

where, $R_{vertical}$ and $R_{horizontal}$ are the means of the experimental values of electrical resistance in the Y- and X-direction, respectively.

Using the known Van der Pauw relation $R_{yy,\square}R_{xx,\square} = R_s^2$ and the $R_{yy,\square}/R_{xx,\square}$ value from (1), the resistances in the two different directions, $R_{xx,\square} = R_{xx}$ and $R_{yy,\square} = R_{yy}$ are obtained. These values were used to calculate the variations of the relative electrical resistance, $\Delta R/R_0 = (R_i - R_{0i})/R_{0i}$ (i = *xx;yy*), and the electrical anisotropy, defined as the electrical resistance ratio ($R_{xx}/R_{yy}$), with the applied deformation during the tensile tests.

### D. Electrical Resistance Results Versus Strain

The knocked down CNT/CFRP samples were strained in parallel (Y), (samples S1 and S2), and transverse (X), (samples T1, T2, and T3), directions with respect to CNT alignment direction, as illustrated in Fig. 2. Note that in the case of the sample S, the strain and opposite directions correspond to Y- and X- directions, respectively, whereas in sample T, the strain and opposite directions correspond to X- and Y- direction, respectively. The samples were subjected to

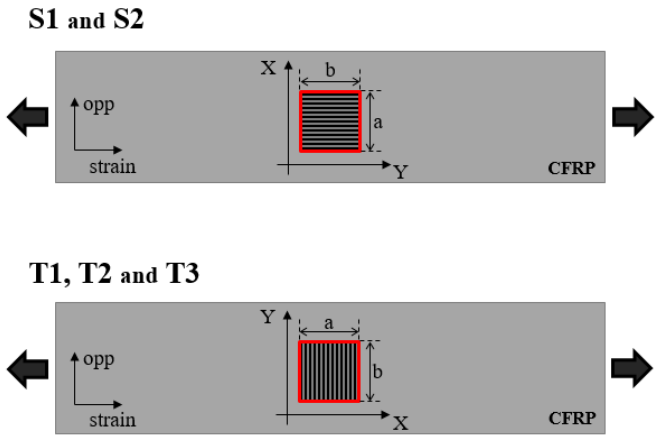


Fig. 2. Schematics of the CNT alignment and patch positions regarding strain direction of samples type S (S1 and S2) and T (T1, T2, and T3).

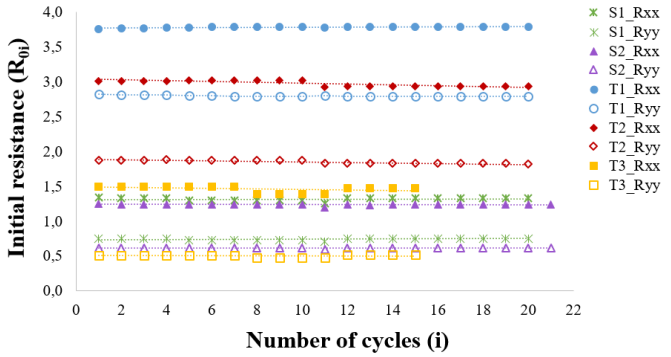


Fig. 3. Variations of the initial electrical resistance values, $R_{0i}$, with the number of cycles (i) for all samples, S1, S2, T1, T2 and T3, in parallel (Y) and opposite (X) direction regarding CNT alignment.

several deformation cycles by an INSTRON 5969 equipped with an optical extensometer to record the longitudinal displacements of the CNT-based sensor during the tensile test. At the end of each cycle, the deformation was reset in a controlled manner/mode lowering the load to zero, with the specimen fixed on the grid.

The relative electrical resistance ($\Delta R/R_0$) and electrical anisotropy ($R_{xx}/R_{yy}$) were obtained for each sample and deformation cycle.

For the tensile tests, tabs were applied to hold the sample on the grips to avoid damages.

## III. Results

### A. Initial Electrical Resistance Results

In the beginning of each deformation cycle, the initial electrical resistance values, $R_{0i}$ (i = cycle number), in parallel (Y) and opposite (X) directions regarding CNT alignment, $R_{yy}$ and $R_{xx}$, respectively, were assessed for each sample. Fig. 3 shows that the variation of $R_{0i}$ values was practically null for all samples in X- and Y-directions, which can be confirmed by the correspondent slopes values presented in Table I. In addition, it is also presented the variations of the average absolute values of the relative initial resistance

TABLE I
Slope Values of the Linear Regression of the $R_{i0}$ in Y- and X-Direction Regarding CNT Alignment (Variations of Fig. 1), and the Average Absolute Values of $R_{0i} - R_{0i=1}/R_{0i=1}$ (i = Cycle Number) for Each Sample

| Sample | Slope of linear regression | | $\overline{((R_{0t} - R_{0t=1})/R_{0t=1})(\%)}$ | |
|---|---|---|---|---|
| | Rxx | Ryy | Rxx | Ryy |
| T1 | 0.0013 | -0.0010 | 0.85 | 0.84 |
| T2 | -0.0059 | -0.0037 | 1.46 | 1.62 |
| T3 | -0.0037 | -0.0003 | 2.58 | 2.50 |
| S1 | 0.0005 | 0.0009 | 1.74 | 1.65 |
| S2 | -0.0007 | 0.0004 | 1.27 | 1.21 |

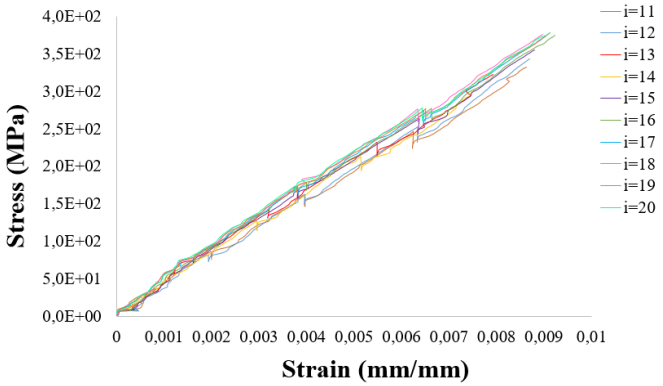


Fig. 4. Stress (MPa) versus Strain (mm/mm) curve for sample tested for ten cycles (i = number of cycles).

TABLE II
Elasticity Modulus Values (E), Their Average ($\bar{E}$) and Standard Deviation ($\sigma$) Values Obtained From the Stress (MPa) Versus Strain (mm/mm) Curves Slope

| Cycle (i) | 11 | 12 | 13 | 14 | 15 | 16 | 17 | 18 | 19 | 20 |
|---|---|---|---|---|---|---|---|---|---|---|
| E (GPa) | 36.1 | 36.2 | 41.5 | 41 | 42.5 | 42.4 | 39.9 | 41.7 | 40.6 | 41.9 |
| $\bar{E}$ (GPa) | 40.4 | | | | | | | | | |
| σ (GPa) | 2.2 | | | | | | | | | |

($R_{0i}$-$R_{0i=1}/R_{0i=1}$) (i = cycle number) for each sample with respect to X- and Y-directions. Overall, all the samples kept their electrical properties, even after 20 deformation cycles.

### B. Mechanical Response

The samples were sequentially strained, and the respective stress-strain curves collected during the several strain cycles (i) are presented in Fig. 4. As shown, the almost linear behavior of the stress-strain curves is reproducible in several cycles (i). The elasticity modulus values, E, obtained from the curves slope are presented in Table II, as well as their average, $\bar{E}$, and standard deviation, $\sigma$. Also, it appears that there is no significant slip of the samples at the holding grips.

### C. Electrical Resistance Results Versus Strain

*1) Strain Direction Parallel to CNT Alignment:* Two samples, S1 and S2, were cyclically strained in parallel direction of

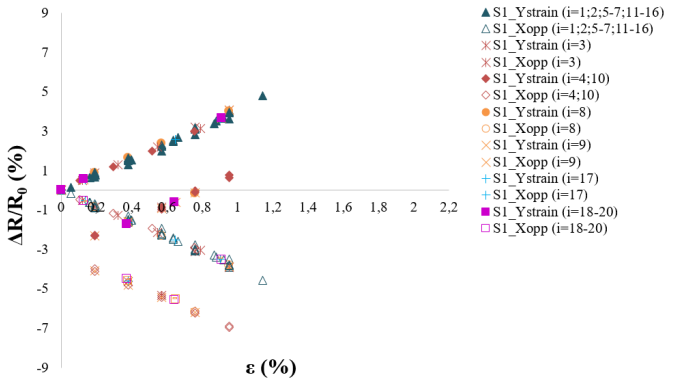


Fig. 5. Variations of the relative electrical resistance ($\Delta R/R_0$) in strain ($Y_{strain}$) and opposite ($X_{opp}$) direction upon cycling deformation of sample S1 (i = number of cycles).

the CNT alignment (Y-direction), and their relative electrical resistance ($\Delta R/R_0$) in strain and opposite directions upon strain increments were studied. In Fig. 5, the $\Delta R/R_0$ values of S1 sample are displayed and grouped by deformation cycles. In general, the $\Delta R/R_0$ values decrease and increase in opposite and strain directions, respectively, however a shifted is observed in some cycles. Thus, to give a clearer vision of the electrical behavior upon strain increments, the curves are presented separately in Fig. 6, highlighting the different obtained behaviors. As shown in Fig. 6-A), the $\Delta R/R_0$ shows a linear behavior for the 1st, 2nd, 5-7th and 11-16th cycles. In 4th, 9th and 10th cycles (Fig. 6-B)), the $\Delta R/R_0$ slope suffers an offset decay while still maintaining its value. Regarding the 8th and 17th cycles (Fig. 6-C)), the $\Delta R/R_0$ has almost a linear behavior, if it was not for the only deviated value at a specific deformation. Finally, the 3rd and 18-20th cycles (Fig. 6-D)) showed a $\Delta R/R_0$ step-like curve, specifically, the slope suffers a shift down, maintained after its previous slope value. Those slightly different electrical behaviors can be attributed to phenomena that occur during cyclical deformation and can interfere with the CNT conductive mechanism by affecting the number of CNT-CNT junctions or CNT-CNT distances. However, these seem to be reversible occurrences since are followed by $\Delta R/R_0$ slope re-establishments, probably due to CNT structural readjustments. Despite all these variations, it is important to clarify that they happen between parallel slopes (represented by the grey lines in Fig. 6) with quite similar values and, given the curve slope is equal to the Gauge Factor (GF), it can be established a steady sensitivity to strain.

As shown in Fig. 7, the S2 sample had quite similar electrical behavior upon cycle deformation, comparing with S1 sample, despite the different values of deformation at break.

In Table III, the detailed analysis of the electrical resistance behavior of S1 and S2 is presented, with the specific $\Delta R/R_0$ slope values (GF) in strain and opposite directions of the curves grouped by deformation cycles (i). These results confirm what visually seemed to be an almost constant GF, despite the observed jumps, indicating a good and steady sensitivity to strain. The GF on the opposite (opp) direction are slightly lower than on the strain direction.

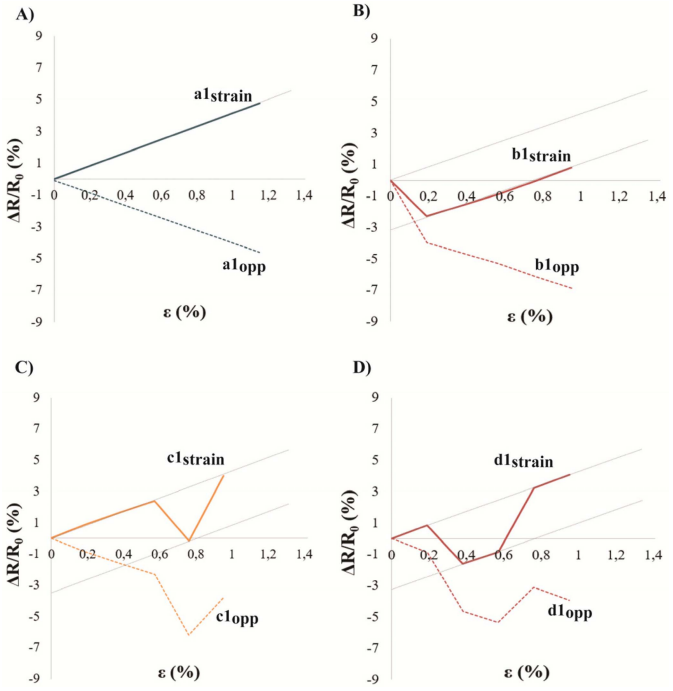


Fig. 6. Relative electrical resistance ($\Delta R/R_0$) behaviour of sample S1 in strain and opposite (opp) directions upon deformation, grouped by cycles: A) 1st, 2nd, 5-7th and 11-16th cycles; B) 4th, 9th and 10th cycles; C) 8th and 17th cycles; D) 3rd and 18-20th cycles.

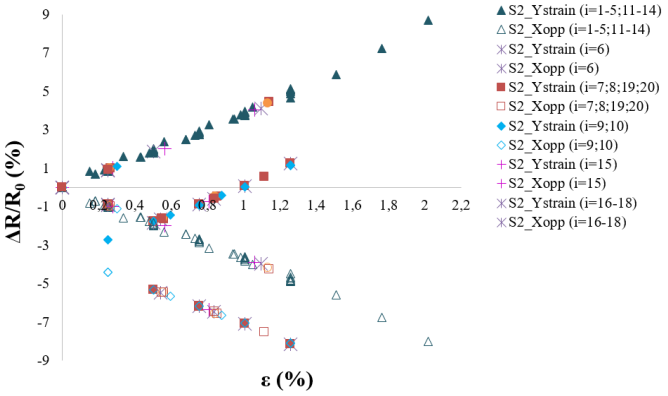


Fig. 7. Relative electrical resistance ($\Delta R/R_0$) in strain ($Y_{strain}$) and opposite ($X_{opp}$) direction upon cycling deformation of sample S2 (i = number of cycles).

The anisotropic electrical behavior of the samples upon strain increments was also analyzed and is presented in Fig. 8. As expected, the anisotropy ($R_{xx}/R_{yy}$) values decrease when the samples, S1 and S2, are strained in parallel direction (Y-direction) regarding CNT alignment (which corroborates with previous work [22]). The results are grouped by cycles due to the slope shifts observed within each sample. The slopes have a constant value, despite the different initial anisotropy values. Moreover, the initial anisotropy values reduce after some cycles. This can be due to network rearrangements that culminate in CNT-CNT accommodation and anisotropy value stabilization. In Table IV, initial $R_{xx}/R_{yy}$ values (zero deformation) for the two samples and respective slopes are

TABLE III
$\Delta R/R_0$ SLOPE VALUES (GF) IN STRAIN AND OPPOSITE DIRECTION OF ALL CURVES GROUPED BY DEFORMATION CYCLES (I) OF SAMPLES S (S1 AND S2) AND T (T1, T2, AND T3)

| Sample | Cycle (i) | Direction | $\Delta R/R_0$ Slope (GF) |
|---|---|---|---|
| S1 | 1; 2; 5-7; 11-16 | Strain | 4.0 |
| | | Opp | -3.9 |
| | 3; 4; 8-10; 17-20 | Strain | 3.9 |
| | | Opp | -3.9 |
| S2 | 1-5; 11-14 | Strain | 4.2 |
| | | Opp | -3.9 |
| | 6-10; 15-20 | Strain | 3.9 |
| | | Opp | -3.5 |
| T1 | 1-3; 5-10 | Strain | 4.5 |
| | | Opp | -4.3 |
| | 4; >11 | Strain | 5.1 |
| | | Opp | -5.0 |
| T2 | 1-10 | Strain | 4.6 |
| | | Opp | -4.3 |
| | >11 | Strain | 4.2 |
| | | Opp | -4.1 |
| T3 | 1; 2; 3; >8 | Strain | 2.9 |
| | | Opp | -2.8 |
| | 4-7 | Strain | 2.6 |
| | | Opp | -2.4 |

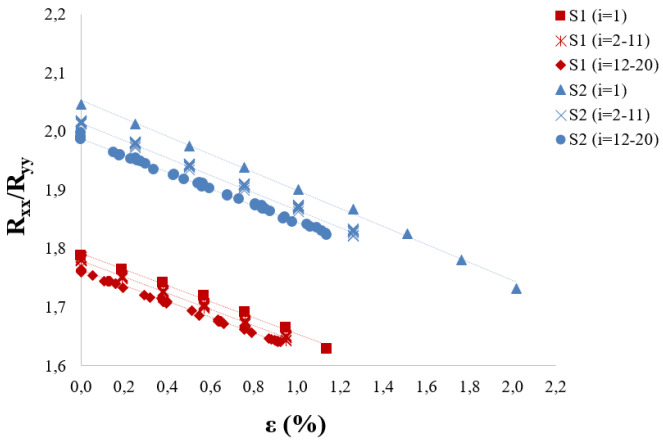


Fig. 8. Electrical anisotropy ($R_{xx}/R_{yy}$) values upon deformation of S1 and S2 samples (i = number of cycles).

presented. The initial values showed a slight variability regarding S1 and S2, probably due to the distinct height and density of the CNT forests used [26]. The linear and constant behavior of the slope values indicates that the electrical anisotropy can be a suitable strain quantifier.

*2) Strain Direction Transverse to CNT Alignment:* In the following Figures, the electrical resistance behavior of the samples T1, T2, and T3, which were strained in opposite

TABLE IV
INITIAL ANISOTROPY VALUES AND RESPECTIVE CURVES SLOPE OF S (S1 AND S2) AND T (T1, T2, AND T3) SAMPLES

| Sample | Cycle (i) | Origin Initial anisotropy | $R_{xx}/R_{yy}$ Slope |
|---|---|---|---|
| S1 | 1 | 1.8 | -0.14 |
| | 2-11 | 1.8 | -0.14 |
| | 12-20 | 1.8 | -0.13 |
| S2 | 1 | 2.1 | -0.16 |
| | 2-11 | 2.0 | -0.15 |
| | 12-20 | 2.0 | -0.14 |
| T1 | 1-3 | 1.4 | 0.13 |
| | >4 | 1.4 | 0.16 |
| T2 | 1; 14 | 1.6 | 0.15 |
| | 2-13; 15-20 | 1.6 | 0.15 |
| T3 | 1-11 | 2.9 | 0.17 |
| | 12-15 | 2.8 | 0.16 |

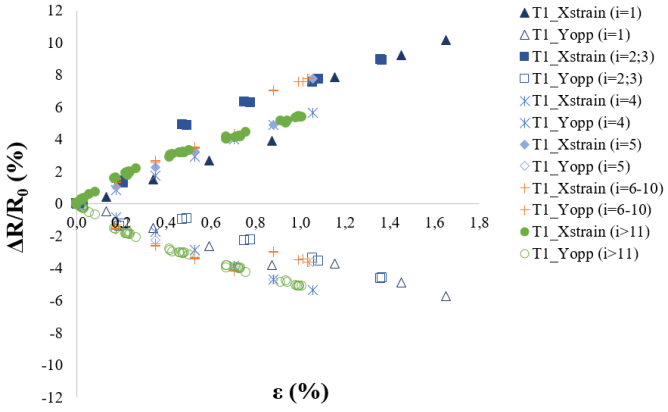


Fig. 9. Relative electrical resistance ($\Delta R/R_0$) in strain ($X_{strain}$) and opposite ($Y_{opp}$) direction upon cycling deformation of sample T1 (i = number of cycles).

direction (X-direction) of the CNT alignment, are presented. Generally, the relative electrical resistance ($\Delta R/R_0$) increases in strain direction and decreases in the opposite one, and it can be observed some variability between samples. The samples T1 (Fig. 9) and T2 (Fig. 10) showed a similar behavior, the linearity of $\Delta R/R_0$ values were affected by small steps at specific deformations. However, after 11 deformation cycles, their electrical behavior was quite constant without slope variations. This may be due to the CNT-CNT structural accommodation, which in these samples have already occurred in the $10^{th}$ cycle.

Regarding the T3 sample (Fig. 11), similarly to the samples S1 (Fig. 5 and Fig. 6) and S2 (Fig. 7) behavior, the $\Delta R/R_0$ slope shifts down maintaining after that its previous slope value in specific deformation cycles (i). As stated above, this can be attributed to some reversible phenomenon that occurs during deformation, interfering with the CNT conductive mechanism. After that, a CNT structural accommodation

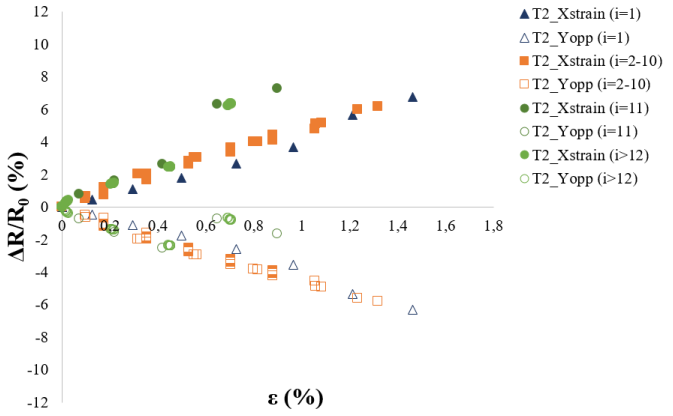


Fig. 10. Relative electrical resistance ($\Delta R/R_0$) in strain ($X_{strain}$) and opposite ($Y_{opp}$) direction upon cycling deformation of sample T2 (i = number of cycles).

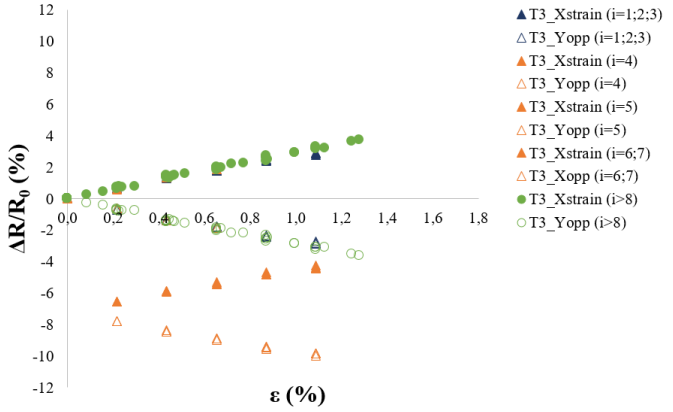


Fig. 11. Relative electrical resistance ($\Delta R/R_0$) in strain ($X_{strain}$) and opposite ($Y_{opp}$) direction upon cycling deformation of sample T3 (i = number of cycles).

seems to happen since the $\Delta R/R_0$ slope is re-established for the following cycles.

In Table III, the $\Delta R/R_0$slope values (GF) of T1, T2, and T3 samples in strain and opposite directions, grouped by deformation cycles, are presented. These results confirm the close similarity between T1 and T2 slope values. Moreover, the Gauge Factor are quite similar for the S1, S2, T1, and T2. However, the values correspondent to T3 are slightly smaller, probably due to the variability of the CNT electrical and structural initial properties. Despite those small disparities, the samples mostly show a high sensitivity to strain and a steady behavior within each sample scope.

In Fig. 12, the anisotropy electrical behavior of the T1, T2, and T3 samples upon strain increments is presented. As expected [22], the anisotropy ($R_{xx}/R_{yy}$) values increase when the samples are strained in opposite direction (X-direction) regarding CNT alignment, presenting a slight variability in the initial values (zero deformation). The results are grouped by cycles due to the slope shifts observed within each sample, specifically, the slope has a constant value but the initial anisotropy value in the beginning of each cycle varies, presenting a constant higher value after some cycles.

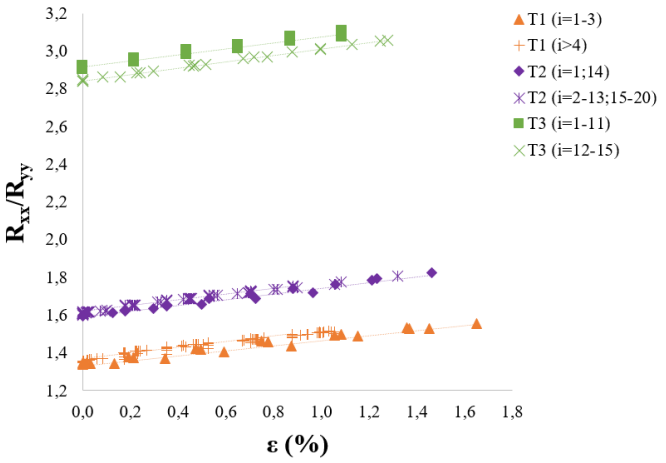


Fig. 12. Electrical anisotropy ($R_{xx}/R_{yy}$) values upon deformation of T1, T2 and T3 samples (i = number of cycles).

As stated earlier, this can be due to network rearrangements that culminate in CNT-CNT accommodation and anisotropy value stabilization. Also, some variability is observed between T1, T2, and T3 initial values, i.e., T3 has significant higher anisotropy values, which can be attributed to CNT intrinsic electrical properties and forests structure [26].

To complement the Fig. 12 analysis, initial $R_{xx}/R_{yy}$ values and respective curves slope are presented for the three samples in Table IV. The similarity of the slope values and the curves linear behavior attest the adequacy of anisotropy as a strain quantifier.

Both types of samples, strained in Y- and X-direction regarding CNT alignment, type S (S1 and S2) and type T (T1, T2, and T3), presented a similar $\Delta R/R_0$slope (Table III), GF=3.9 ± 0.2; 3.9 ± 0.9, respectively, despite the jumping effects with the strain and number of cycles. The number of cycles needed to reach a steady state, and the linear slope can depend on the electrical and structural initial properties of the CNT forest used in the samples' preparation, thus the dissimilar electrical behavior in some cycles. The absolute electrical resistance anisotropy ($R_{xx}/R_{yy}$) values variation were quite close for all samples and showed high linearity, which can be represented by:

$$R_{xx}/R_{yy}\,(\epsilon) = \left(R_{xx}/R_{yy}\right)_0 \pm S\varepsilon \tag{3}$$

where, $\left(R_{xx}/R_{yy}\right)_0$ is the initial electrical resistance anisotropy, S is a strain-sensitivity factor and $\varepsilon$ the strain. The ± sign depends upon the direction of strain with respect to the alignment of the CNT: positive if the strain direction is transverse to CNT alignment; and negative in the opposite case. This opposite behavior of the electric resistance anisotropy when the samples are strain in different directions regarding CNT alignment can be used as, not only a strain quantifier, but also as a strain direction indicator [22].

## IV. Conclusion

In this work, a proof of concept of an aligned CNT based strain sensor for structural health monitoring is presented.

The CNT sensing patch was placed on the surface of a conventional aeronautic laminate considering two different alignment directions, i.e., CNT alignment parallel (Y) and transversal (X) to strain direction. The electrical response of these two type of sensors, type S and type T, respectively, was thoroughly evaluated during cyclic deformation. The initial electrical values presented some variability owing to the electrical and structural initial properties of the CNT forest.

In general, their $\Delta R/R_0$ increased and decreased in strain and opposite directions, respectively, and showed steady and similar gauge factor values. Despite, some electrical resistance behavior disparities were observed in specific cycles that are probably caused by phenomena that interfere with the CNT conductive mechanisms during deformation (e.g., changes on the number of CNT-CNT junctions or distances). These occurrences seem to be quite reversible since a $\Delta R/R_0$ slope re-establishment is observed, most likely due to CNT structural readjustment.

The electric resistance anisotropy showed linear and steady slopes during cyclic deformation. Moreover, its opposite behavior when the samples are strain in different directions regarding CNT alignment can be used as strain direction indicator.

Not only it has been proved that this aligned CNT-based sensor is suitable for strain quantification, but also as a strain direction indicator, being a substantial asset for structural health monitoring.

## REFERENCES


[1] L. Gao, E. T. Thostenson, Z. Zhang, and T.-W. Chou, "Sensing of damage mechanisms in fiber-reinforced composites under cyclic loading using carbon nanotubes," *Adv. Funct. Mater.*, vol. 19, no. 1, pp. 123–130, Jan. 2009.

[2] R. Balaji and M. Sasikumar, "Structural health monitoring (SHM) system for polymer composites: A review," *Indian J. Sci. Technol.*, vol. 9, no. 41, pp. 1–12, Nov. 2016.

[3] A. Santos, L. Amorim, J. P. Nunes, L. A. Rocha, A. F. Silva, and J. C. Viana, "A comparative study between knocked-down aligned carbon nanotubes and buckypaper-based strain sensors," *Materials*, vol. 12, no. 12, p. 2013, Jun. 2019.

[4] X. Wang, S. Lu, K. Ma, X. Xiong, H. Zhang, and M. Xu, "Tensile strain sensing of buckypaper and buckypaper composites," *Mater. Des.*, vol. 88, pp. 414–419, Dec. 2015.

[5] M. D. Rein, O. Breuer, and H. D. Wagner, "Sensors and sensitivity: Carbon nanotube buckypaper films as strain sensing devices," *Compos. Sci. Technol.*, vol. 71, no. 3, pp. 373–381, Feb. 2011.

[6] S. Lu *et al.*, "Monitoring the manufacturing process of glass fiber reinforced composites with carbon nanotube buckypaper sensor," *Polym. Test.*, vol. 52, pp. 79–84, Jul. 2016.

[7] T. Xu, Q. Qiu, S. Lu, K. Ma, and X. Wang, "Multi-direction health monitoring with carbon nanotube film strain sensor," *Int. J. Distrib. Sensor Netw.*, vol. 15, no. 2, Feb. 2019, Art. no. 155014771982968.

[8] N. T. Selvan *et al.*, "Piezoresistive natural rubber-multiwall carbon nanotube nanocomposite for sensor applications," *Sens. Actuators A, Phys.*, vol. 239, pp. 102–113, Mar. 2016.

[9] L. Vertuccio, L. Guadagno, G. Spinelli, P. Lamberti, V. Tucci, and S. Russo, "Piezoresistive properties of resin reinforced with carbon nanotubes for health-monitoring of aircraft primary structures," *Compos. B, Eng.*, vol. 107, pp. 192–202, Dec. 2016.

[10] Q. Li *et al.*, "Engineering of carbon nanotube/polydimethylsiloxane nanocomposites with enhanced sensitivity for wearable motion sensors," *J. Mater. Chem. C*, vol. 5, no. 42, pp. 11092–11099, 2017.

[11] Y. Gao, X. Fang, J. Tan, T. Lu, L. Pan, and F. Xuan, "Highly sensitive strain sensors based on fragmentized carbon nanotube/polydimethylsiloxane composites," *Nanotechnology*, vol. 29, no. 23, Jun. 2018, Art. no. 235501.

[12] E. J. Garcia, B. L. Wardle, and A. J. Hart, "Joining prepreg composite interfaces with aligned carbon nanotubes," *Compos. A, Appl. Sci. Manuf.*, vol. 39, no. 6, pp. 1065–1070, Jun. 2008.

[13] M. K. Shin, J. Oh, M. Lima, M. E. Kozlov, S. J. Kim, and R. H. Baughman, "Elastomeric conductive composites based on carbon nanotube forests," *Adv. Mater.*, vol. 22, no. 24, pp. 2663–2667, May 2010.

[14] A. M. Amani, S. A. Hashemi, S. M. Mousavi, H. Pouya, and V. Arash, "Electric field induced alignment of carbon nanotubes: Methodology and outcomes," in *Carbon Nanotubes—Recent Progress*. U.K.: IntechOpen, 2018, p. 71.

[15] A. I. Oliva-Avilés, F. Avilés, V. Sosa, A. I. Oliva, and F. Gamboa, "Dynamics of carbon nanotube alignment by electric fields," *Nanotechnology*, vol. 23, no. 46, Nov. 2012, Art. no. 465710.

[16] D. J. Lipomi *et al.*, "Skin-like pressure and strain sensors based on transparent elastic films of carbon nanotubes," *Nature Nanotechnol.*, vol. 6, no. 12, pp. 788–792, Dec. 2011.

[17] S. Li, J. G. Park, S. Wang, R. Liang, C. Zhang, and B. Wang, "Working mechanisms of strain sensors utilizing aligned carbon nanotube network and aerosol jet printed electrodes," *Carbon*, vol. 73, pp. 303–309, Jul. 2014.

[18] L. Zhang, G. Zhang, C. Liu, and S. Fan, "High-density carbon nanotube buckypapers with superior transport and mechanical properties," *Nano Lett.*, vol. 12, no. 9, pp. 4848–4852, Sep. 2012.

[19] A. Li, A. E. Bogdanovich, and P. D. Bradford, "Aligned carbon nanotube sheet piezoresistive strain sensors," *Smart Mater. Struct.*, vol. 24, no. 9, Sep. 2015, Art. no. 095004.

[20] J. Lee, I. Y. Stein, S. S. Kessler, and B. L. Wardle, "Aligned carbon nanotube film enables thermally induced state transformations in layered polymeric materials," *ACS Appl. Mater. Interfaces*, vol. 7, no. 16, pp. 8900–8905, Apr. 2015.

[21] N. E. Boyer, "Microfabrication with smooth, thin CNT/polymer composite sheets," M.S. thesis, Dept. Phys. Math. Sci., Phys. Astron., Brigham Young Univ., Provo, UT, USA, 2016.

[22] A. Santos, L. Amorim, J. P. Nunes, L. A. Rocha, A. F. Silva, and J. C. Viana, "Aligned carbon nanotube based sensors for strain sensing applications," *Sens. Actuators A, Phys.*, vol. 289, pp. 157–164, Apr. 2019.

[23] C. A. Coelho, A. T. Sepúlveda, L. A. Rocha, and A. F. Silva, "Carbon nanotubes—The challenges of the first syntheses trials," in *Proc. Int. Conf. Biomed. Electron. Devices*, 2015, pp. 95–102.

[24] J. D. Wasscher, "Note on four-point resistivity measurements on anisotropic conductors," *Philips Res. Rep.*, vol. 16, no. 4, pp. 301–306, 1961.

[25] I. Kazani *et al.*, "Van Der Pauw method for measuring resistivities of anisotropic layers printed on textile substrates," *Textile Res. J.*, vol. 81, no. 20, pp. 2117–2124, Dec. 2011.

[26] J. Lee *et al.*, "Impact of carbon nanotube length on electron transport in aligned carbon nanotube networks," *Appl. Phys. Lett.*, vol. 106, no. 5, 2015, Art. no. 053110.


**Ana Raquel Santos** received the M.Sc. degree in biomedical engineering from FCT/UNL, Portugal, in 2016. Her master's degree dissertation was on biomaterials area: "Development of conductive membranes based on chitosan and reduced graphene oxide for biomedical applications."

From 2016 to 2019, she was a Researcher in the Introduction of Advanced Materials Technologies Into New Product Development for the Mobility Industries (IAMAT) Project with the University of Minho, Portugal, in which her work was focused on CNT-based strain sensor development. She is currently a Researcher with the Institute for Polymers and Composites (IPC), University of Minho, under the Science DiabetICC Footwear Project, where she is developing pressure, temperature, and humidity sensors for an insole with therapeutic applications.

**Luís Amorim** received the master's degree in polymer engineering from the University of Minho, worked on thermoplastic matrix composites production optimization, "towpregs," where he is pursuing the Ph.D. degree with the Institute of Polymers and Composites.

After two years as an Extrusion Process Engineer at BOPP Film Company, he joined a research team to develop composites pressure vessels for commercial applications. He is currently a Researcher with the Introduction of Advanced Materials Technologies Into New Product Development for the Mobility Industries (IAMAT) Project for studying and understanding the impact of damage mechanisms in advanced composites for aeronautic applications in order to improve their resistance.

**João Pedro Nunes** received the degree in mechanical engineering from the Faculty of Engineering, University of Porto, in 1981, and the M.Sc. (SMC rheology) and Ph.D. (development of new thermoplastic matrix composites) degrees in polymer science and engineering from the University of Minho, in 1992 and 1998, respectively.

He began his career as a Technical Manager with the Portuguese composite manufacturer Vidropol. After six years of industrial experience, he became a Junior Lecturer with the Department of Polymer Engineering, University of Minho, in 1988. From 2000 to June 2015, he was the Director of Engineering with the Portuguese SME manufacturer VIDROPOL and began his career as a Private Consultant of the composite industry. He has been the Director of the Doctoral Program in Science and Engineering of Polymers since 2011. Since 2019, he has also been an Executive Director of the Innovation Centre in Polymer Engineering (PIEP), University of Minho, where he has been the Scientific Coordinator of the Composite Materials Area since 2012. He was the Deputy Director of the Department of Polymer Engineering from March 2017 to March 2019. He is an Auxiliary Professor with the Department of Polymer Engineering and a Senior Researcher with the Institute for Polymers and Composites (IPC), University of Minho/Portugal. He participated in more than 30 European and national research and development projects, mainly, related to the development of new cost-effective composites and processing technologies. He has authored or coauthored nine book chapters and more than 100 articles in international journals. He has nine patents (five international and four national) registered in his name and received two awards (one international and the other national).

**Alexandre F. Silva** received the M.Sc. degree in biomedical engineering and the Ph.D. degree in engineering design and advanced manufacturing under the Leaders for Technical Industries Program from the University of Minho (UMinho), Braga, Portugal, in 2007 and 2011, respectively.

He is currently an Invited Assistant Professor with the Department of Industrial Electronics, University of Minho, where he has been developing research in the field of instrumentation and electronic microsystems.

**Júlio C. Viana** received the bachelor's degree in industrial engineering–plastics branch from the University of Minho in 1991, the M.Sc. degree in computer aided engineering–mechanical design from Queen's University Belfast, U.K., in 1993, and the Ph.D. degree in science and engineering of polymers and composites from the University of Minho in 2000.

In 1991, he joined the University of Minho as a Professor, where he is currently an Associate Professor with the Department of Polymer Engineering. He is also the Director of the Institute for Polymers and Composites (IPC) Research Unit, University of Minho. His research interests include advanced polymer systems and manufacturing technologies, flexible electronics, and smart polymeric products.